Non-Traditional Cell Geometry for Improved Copper Plating Uniformity

Holly Garich,[a,*] Sirivatch Shimpalee,[b,*] Visarn Lilavivat,[c] Stephen Snyder,[a,*] and E. J. Taylor[a,*,z]

[a]*Faraday Technology, Inc., Englewood, Ohio 45315, USA*
[b]*Department of Chemical Engineering, University of South Carolina, Columbia, South Carolina 29208, USA*
[c]*National Metal and Materials Technology Center, Pathum Thani 12120, Thailand*

Many factors contribute to uniform electrochemical processing in industrial applications. The electrochemical cell provides the foundation for the process and as such an effective geometry is critical to obtain desired properties and to maximize process efficiency. A non-traditional cell geometry has been engineered to provide a uniform boundary layer thickness to dampen uneven localized current distributions and promote consequent plating uniformity for full size printed circuit board panels. This tank has been extensively characterized for thickness distribution under direct current plating conditions and compared with commercial plating cell geometries that utilize both educator flow and/or air sparging agitation. Compared to the conventional cells, the variation of copper deposit thickness across the panel in the non-traditional is significantly less, and meets the requirement of the printed circuit board industry. Cell geometry, panel features and operating parameters have been modeled and show good agreement with experimental data. The results of this study suggest that through hole patterns on a printed circuit board increase the non-uniformity of the boundary layer thickness.

Manuscript submitted April 21, 2016; revised manuscript received May 17, 2016. Published May 24, 2016.

In the manufacture of printed circuit boards (PCBs), copper electrodeposition plays an important role in the final product's reliability and performance. Deposits that are non-uniform may induce reliability issues and ultimately hamper device performance. Furthermore, copper deposits with columnar grain structures are prone to cracking and may result in device failure. As such, implementation of a robust process that provides high levels of uniformity and the desired grain structure promotes higher throughput and higher quality products, decreasing manufacturing costs.

Processing conditions such as agitation mechanism, electrolyte composition and electric field parameters control the properties of copper deposits as well as governing the uniformity of metallization over the PCB surface. Conventionally, much emphasis has been placed on electrolyte composition, specifically use of organic additives (in parts-per-million (ppm) concentrations), as a means to help control copper deposit uniformity and improve throw/fill within the micron size features. However, regardless of the electrolyte composition used, optimization of the plating cell geometry and agitation mechanism may greatly enhance the uniformity achieved in the copper electrodeposition process.

In traditional plating cells, air sparging, and more recently eductor flow, is used as the primary agitation mechanism. Other agitation schemes (lateral oscillation, knife-edge oscillation and vibration of the panel) have been added in attempts to achieve a time averaged boundary layer thickness, which yields uniform current distribution and consequently uniform plating thicknesses. Another technology for controlling solution flow in a plating cell uses a paddle to create a turbulent wave of electrolyte that moves back and forth across the surface of the workpiece,[1] in an attempt to create a time average dynamic flow to create uniform hydrodynamic conditions. However, the wave cannot move fast enough to maintain a uniform boundary layer across the entire surface of the workpiece at a given time.

Non-traditional plating cell geometries provide a path for improved processing capabilities despite electrolyte compositions. Furthermore, plating cells that demonstrate a uniform boundary layer thickness would provide ease in development of pulse/pulse reverse electric field processing conditions, which depend on boundary layer thickness and feature size. In this paper, characterization of a non-traditional plating cell geometry[2–5] demonstrates that through improvements in the agitation mechanism, a boundary layer of uniform thickness is delivered to the substrate and this results in a highly uniform copper deposit thickness. Thickness distribution experiments were conducted on traditional plating cell geometries and are compared to the performance in the non-traditional cell. The boundary layer thickness in the non-traditional cell was experimentally approximated and the resulting thickness distribution confirmed under different flow regimes. Modeling work was conducted to approximate the boundary layer thickness achieved under varying plating conditions, and comparison with experimental results show an excellent match between simulation and experimentally derived values.

Experimental

Electrolyte flow control.—Electrolyte agitation is a significant factor in the uniformity of metallization of PCBs. In conventional plating tank designs, electrolyte flow is often facilitated by air sparging or by eductors placed in an impinging or glancing orientation with respect to the substrate. Eductors placed in an impinging or glancing orientation result in non-uniform flow profiles and consequent non-uniform boundary conditions, as depicted in Figure 1.[6–8]

In the non-traditional cell, the substrate (cathode) is positioned in the center of two stationary anode chambers (Figure 2). The anode to cathode spacing ranges from 16.5 to 30 cm. A polymeric cloth is stretched and secured to the front of each anode chamber with a polypropylene frame, forming a surface that impedes solution flow but not current flow. The coupling of the polymeric cloth and anode chamber forms distinct flow channels on either side of the substrate. Each anode chamber houses four titanium baskets, which are covered in polypropylene bags and filled with phosphorized copper anode balls (2.5 cm diameter Cu-Phos, Univertical, Angola, IN). Insulating shields to control current distribution are attached to the anode chamber as needed.

Flow in the tank is achieved by pumping electrolyte through six, 1.9 cm eductors (Ser-Ductor, Serfilco) located on the bottom of the tank, with three eductors positioned below each anode chamber. Flow from the eductors hits a dampening element, which directs the flow in a parallel fashion with respect to the substrate, as indicated by the arrows in Figure 2. Flow through each set of three eductors is controlled separately, and as such alternating flow regimes may be utilized. The flow rate from each pump to the eductors is up to 3.8 L/s per side. Additional agitation of the electrolyte-substrate interface is achieved via lateral oscillation with stroke of 2.5 cm and 0–1.1 cycles/s, and vibration of the substrate at 0–36 cycles/s.

*Electrochemical Society Member.
[z]E-mail: jenningstaylor@faradaytechnology.com

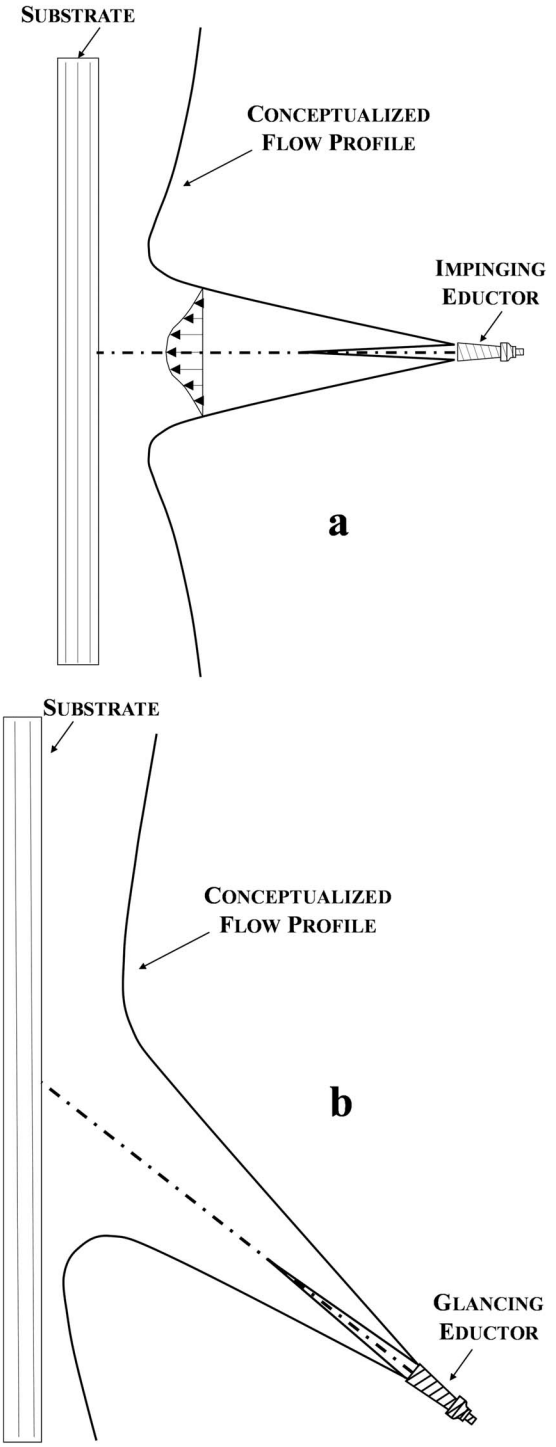

Figure 1. Conceptual flow profiles resulting from a) impinging eductors with respect to the substrate surface and b) glancing eductors with respect to the substrate surface.

Thickness distribution characterization.—Copper foils were deposited on flat stainless steel panels (46 cm × 61 cm) in the non-traditional cell under direct current (DC) conditions in a low additive, acid copper electrolyte comprised of: 95–100 g/L $CuSO_4 \cdot 5H_2O$ (Maxi-Pure, Univertical, Angola, IN), 210–215 g/L H_2SO_4 (Technical Grade, Chemical Services, Dayton, OH), 60–70 ppm Cl^- (as HCl, reagent grade) and 350 ppm polyethylene glycol (~3350 MW, Sigma Aldrich). The substrates were plated using either a Hendor Model pe86D-6-212-480 or an American Plating Power A1D-400/400

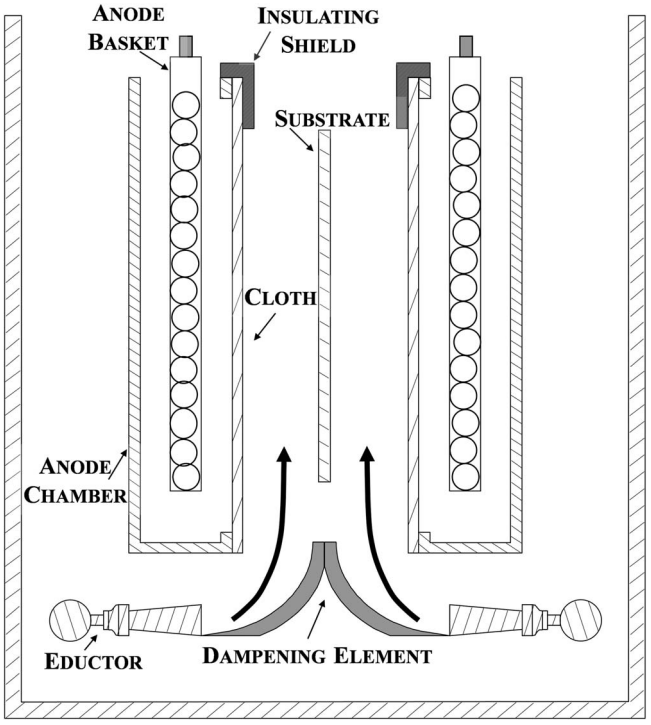

Figure 2. Cross-sectional view of the non-traditional plating cell geometry utilizing parallel solution flow with respect to the substrate surface. Parallel flow is achieved through orienting the eductors below each anode chamber and directing flow to the substrate surface with the dampening element; distinct flow channels are formed between the substrate and the anode chambers.

MV24-G4 rectifier. Plating experiments were conducted for 60 minutes and thus the thickness of the deposited copper foils varied with current density. Thickness measurements of the foils were taken 38 mm from all four edges (Figure 3) using a micrometer (Mitutoyo Model 331-261 IP 65 Coolant Proof digimatic micrometer; accuracy ± 2 μm) after each foil was peeled from the stainless steel substrate, and a coefficient of variation was calculated to quantify the degree of

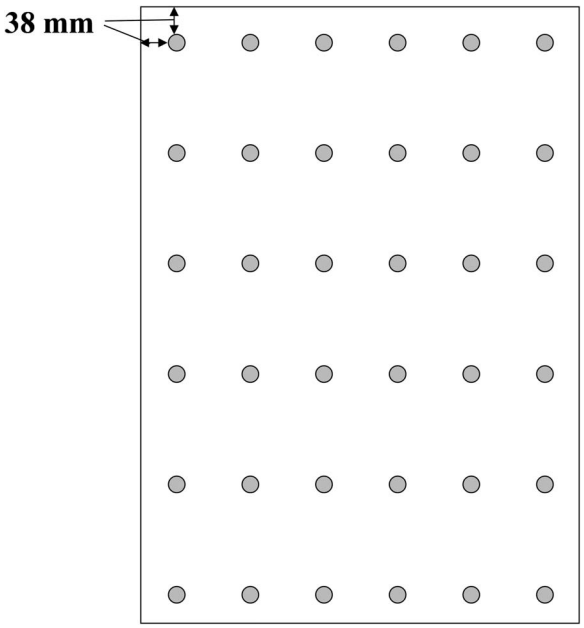

Figure 3. Measurement scheme for copper thickness distribution experiments.

Table I. Thickness distribution as a function of cell geometry in the non-traditional and conventional cells.

Cell Geometry/Cell Attributes	CV (%)
Non-traditional cell:	
191 mm top only insulating shields. Pump flow = 3.8 L/s.	5.3
14″ × 18″ frame shield. Pump flow = 3.8 L/s.	6.5
191 mm top only insulating shields, without polymeric cloth. Pump flow = 3.8 L/s.	9.2
Without shielding - anode chambers and cloth only. Pump flow = 3.8 L/s.	10
Without shields, anode chambers, or polymeric cloth. Pump flow = 3.8 L/s.	14
Air sparging only	14
Conventional Cells:	
Conventional Cell 1: Glancing eductors (25–30°) and air sparging.	31
Conventional Cell 2: Glancing and impinging eductors on bottom and sides of tank.	19
Conventional Cell 3: Impinging eductors on bottom of tank	25–30

thickness variation across the foil. Thickness distribution was evaluated experimentally as a function of cell geometry, flow rate and current density. Thickness distribution tests were also conducted in three conventional cells, which utilize air sparging and/or impinging and glancing eductors (Table I). Standard plating conditions such flow rate and anode-to-cathode spacing were maintained for each test; thickness distribution tests were conducted using a DC current density of 27 mA/cm^2 for 60 minutes. Coefficient of variation values were calculated for each conventional cell test and compared to that obtained with the non-traditional cell geometry.

Boundary layer characterization.—The boundary layer thickness was calculated from the limiting current approximated from linear polarization curves (EG&G PAR Model 273A Potentiostat and EG&G PAR Model 352/252 SoftCorr II software) in the method outlined by Wu et al.[9] Linear polarization curves were measured in a dilute copper electrolyte (7.6–7.9 g/L $CuSO_4 \cdot 5H_2O$, 93 g/L H_2SO_4, 1.2 ppm Cl^- as HCl) using a three electrode configuration. Flat stainless steel substrates (31 cm × 46 cm; 46 cm × 61 cm; 50 cm × 50 cm, masked to 5 cm^2) functioned as the working electrode, a saturated calomel electrode (SCE) functioned as the reference electrode and the anode functioned as the auxiliary electrode (copper bus bar supporting titanium baskets filled with phosphorized copper balls (2.5 cm diameter Cu-Phos, Univertical, Angola, IN) housed in polypropylene bags). Copper clips connected to the copper bus bar (auxiliary) and cathode bus bar (working) facilitated the electrical connections; the reference electrode was supported on the cathode bus bar and placed as close as possible to the exposed area on the stainless steel panel. Flow perturbations caused noise in the linear polarization scan from which the limiting current was approximated.

Linear polarization scans were run with a 10 mV/s scan rate and a 0–1 V range. Boundary layer conditions were assessed as a function of 1) flow rate (0–3.85 L/s), 2) lateral oscillation rate (0–1 oscillation/s), 3) vibration frequency (0–35 cycles/s), as well as 4) location on the panel (shown schematically in Figure 4). The boundary layer calculations were performed per Equation 1:

$$\delta_N = \frac{nFADC_b}{i_L} \quad [1]$$

where n is the number of electrons transferred, F is Faraday's constant (96487 C/mol), A is the area (m^2), D is the diffusion coefficient of copper ion (5.37×10^{-10} m^2/s), C_b is the bulk concentration of copper ion (mol/m^3) and i_L is the limiting current (A). In general, multiple scans (three to four) were conducted for each set of test conditions and average calculated boundary layer thicknesses are reported. Flow rates are measured with non-contact, ultrasonic flow transducers with digital read-out; the system utilizes two transducers, one for each pump.

Modeling of the boundary layer conditions.—From a manufacturing standpoint, it is important to consider how the distribution and density of PCB features influences boundary layer conditions. A model was developed to assess the impact plated through hole (PTH) density imparts on the uniformity of the boundary layer in the non-traditional plating cell. The first step in this process was to develop a preliminary model that predicts the boundary layer conditions within the non-traditional cell. The computational fluid dynamics technique (Star-CD version 4.18) with user defined subroutine that accounts for the physic of electrochemical plating was used to simulate the flow behavior within the non-traditional cell and predict boundary layer thickness under standard plating conditions from a low-additive, sulfuric acid copper electrolyte. The plating conditions assumed as input parameters for model development are pump flow rate = 3.8 L/s; oscillation = 23 cycles/s; lateral oscillation = 0.43 cycles/s; anode to cathode spacing = 21.3 cm; insulating shields = 19.1 cm top only. The numerical procedure utilized the Computational Continuum Mechanics (CCM) method and assumes parallel flow with respect to the substrate, buoyancy driving flow, steady state calculations and a user-defined subroutine for electrochemical calculations.

The model was initially developed to predict the boundary layer thickness resulting from a flat substrate and evaluated the same locations as used for linear polarization scans (Figure 4). Model refinement was centered on evaluating the boundary layer thickness resulting from varying PTH pattern densities on PCB panels. This model utilized a PTHs density input of 195 holes/5.14 cm^2 (densities of 100 and 195 holes/5.14 cm^2 area were initially evaluated) and PTH diameter of 0.05 cm (0.025, 0.05 and 0.1 cm were initially evaluated).

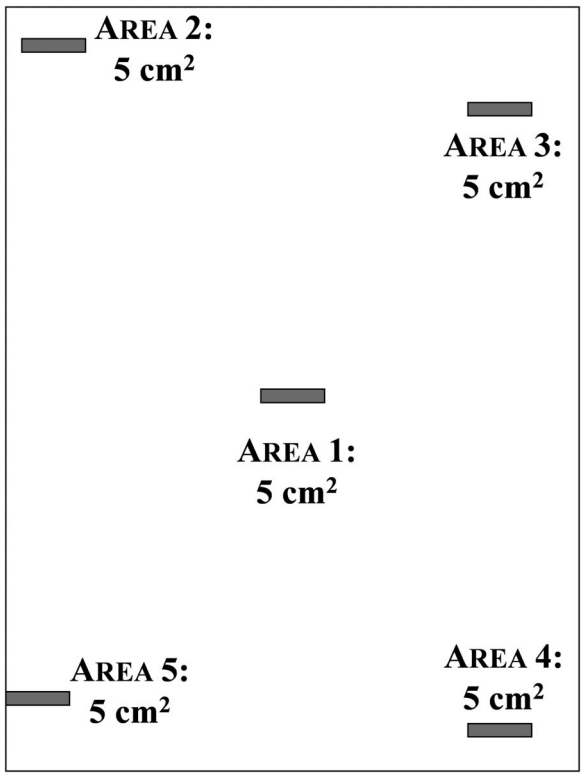

Figure 4. Locations on a 46 cm × 61 cm stainless steel panel indicating exposed area used for polarization curves and subsequent calculation of the boundary layer thickness achieved in the non-traditional plating cell.

Table II. Thickness distribution of copper electrodeposits plated as a function of flow rate, current density and insulation shield dimensions in the non-traditional cell.

Test Number	Current Density (mA/cm^2)	Flow Rate (L/s)	Anode Opening (cm × cm)	CV (%)
CV-1	16	0.95	53 × 64	9.0
CV-2	16	3.8	53 × 64	15
CV-3	16	3.8	36 × 46	15
CV-4	27	0.95	36 × 46	7.5
CV-5	27	0.95	53 × 64	17
CV-6	27	0.95	53 × 58	9.8
CV-7	27	0.95	53 × 75	24
CV-8	27	3.8	36 × 46	6.5
CV-9	27	3.8	53 × 58	12
CV-10	27	3.8	53 × 64	5.3
CV-11	27	3.8	53 × 75	9.9
CV-12	32	3.8	36 × 46	8.2
CV-13	32	3.8	53 × 58	8.6
CV-14	32	3.8	53 × 64	8.9

Results and Discussion

Thickness distribution of copper electrodeposits in the non-traditional cell.—Experimental work on flat panels indicates that the components of the non-traditional cell work in a synergistic manner to promote deposit uniformity. As seen in Table I, operating the cell without the use of the anode chambers and/or polymeric cloth worsens the thickness distribution as evidenced by the coefficient of variation (CV). The flow was observed to be much less controlled without the polymeric cloth and especially without the anode chambers. The optimized configuration of the cell results in a low variation (∼5%) of the deposited thickness across the surface of a 46 cm × 61 cm flat panel, which is anticipated to promote PCB reliability.

The thickness distribution in the cell was also evaluated as a function of flow rate and current density. The results of this work are summarized in Table II for 46 cm × 61 cm flat panel substrates. Deposits with low thickness distribution (i.e. low CV values) may be obtained under a variety of current densities and flow rates in the non-traditional cell. In general, increasing the flow rate improves the thickness distribution across the panel surface and increasing the current density worsens deposit uniformity, though this is dependent on processing conditions. If low flow rates (0.95 L/s) are to be utilized for high current densities (27–32 mA/cm^2), the appropriate insulating shields should be used in the cell, otherwise dark, powdery and non-adherent deposits (commonly referred to as burning) are obtained, especially along the top edge and sides of the panel. If insufficient agitation is supplied, especially in high current density areas, the copper ions for reduction are depleted faster than they are replenished and hydrogen evolution dominates. It is interesting to note that when employing a flow rate of 0.95 L/s, the thickest portion of the deposit occurs at the top of the panel as well as the sides, depending on the shielding used. Conversely, when employing a flow rate of 3.8 L/s, the thickest portion of the panel occurs at the bottom or sides. High current densities (27–32 mA/cm^2) may be employed while maintaining good uniformity (CV ≤10%) if moderate to high flow rates are used (≥1.5 L/s); this study only included a limited number of data points at the lowest current density (16 mA/cm^2) since manufacturing considerations drive processes to the fastest possible metallization rate while maintaining acceptable uniformity.

As with other plating geometries, the use of insulating shields may be used in the non-traditional cell to address plating non-uniformities that inherently arise with necessary deviations from the standard plating conditions (most notably panel size, flow rate, and/or current density), commonly encountered in PCB manufacturing. By selecting the appropriate shielding dimension, copper thickness uniformity is maintained. In the non-traditional cell, the frame securing the polymeric cloth on the anode chamber acts as an insulating shield. However, additional insulating shields may further improve uniformity by either fitting on the top of the anode chamber to shield the top portion of the panel or sliding inside the anode chamber for frame-style shielding that incorporates both top and side shielding to the panel. Addition of the frame-style insulating shield to the interior of the anode chamber ensures that the insulating frame will not interfere with the flow delivered to the PCB; the dimensions listed for the frame-style shielding indicates the dimensions of the open area (covered in the polymeric cloth). Four shielding configurations were evaluated, no shielding (open area of 53 cm × 75 cm), top only shielding of 19 cm (open area 53 cm × 64 cm), top shielding of 24 cm (open area of 53 cm × 58 cm) and a frame shield with open area of 36 cm × 46 cm. Results from thickness distribution tests exploring the impact of insulating shield dimension on CV are summarized in Table II. It is apparent that the appropriate set of shields should be based on the applied current density and flow rate. For example, when deposits were plated at 27 mA/cm^2 using flow rates of 0.95 L/s and a top shield of 19 cm, (test #CV-5) burning on the top edge of the panel was observed along with a high thickness distribution (CV = 17%). When the top shielding is expanded to 24 cm, the burning at the top of the panel is eliminated and a lower CV value is obtained (test #CV-6 = 9.8%). When plating at 27 mA/cm^2 with a flow rate of 0.95 L/s, the thickness distribution may be lowered further by shielding the sides of the panel with frame style shielding (test #CV-4 = 7.5%). The uniformity may then be further improved by increasing the flow rate from 0.95 L/s to 3.8 L/s (test #CV-8 = 6.5%).

Boundary layer thickness measurements.—The agitation mechanism coupled with the geometry of a plating cell will govern the boundary layer conditions. Table III shows the calculated boundary layer thickness from linear polarization curves generated in the non-traditional cell as a function of flow rate under standard plating conditions (0.4 oscillation/s, 20 cycles/s vibration and substrate dimensions of 46 cm × 61 cm). As seen in Table III, there is a decrease in the boundary layer thickness from 23 μm to 10 μm when increasing the volumetric flow rate from zero to 3.8 L/s, under standard oscillation and vibration conditions. When the system is under conditions of zero agitation (no flow, no oscillation and no vibration), a boundary layer thickness of 68 μm is calculated. Furthermore, it was observed that an oscillation rate of 0.4 oscillations/s and a vibration frequency of 20 cycles/s resulted in the lowest boundary layer thickness (tested at pump flow rates of 2.2 and 3.8 L/s) (Table IV) for 46 cm × 61 cm panels. These values have been previously used as standard plating conditions due to uniformity tests conducted in the non-traditional cell (3). These tests also demonstrate that the change in boundary layer thickness at varying oscillation and vibration frequencies is less pronounced when testing at the higher flow rate (3.8 L/s) and that utilization of vibration agitation in conjunction with flow has slightly more impact at thinning the boundary layer when compared to oscillation agitation coupled with flow (these observations hold for all substrate dimensions tested). This series of tests also demonstrated that panel size has little impact on the thickness of the boundary layer in the non-traditional cell under the conditions of standard agitation and varied flow rate (Table V). The boundary conditions achieved under each flow regime show the same boundary layer conditions regardless of panel size in the non-traditional cell.

Table III. Experimentally calculated boundary layer thickness as a function of flow rate on a 46 cm × 61 cm flat stainless steel substrate in the non-traditional cell. Location 1 on the panel.

Pump Flow Rate (L/s)	Osc (osc/s)	Vib (cycles/s)	Ave δ (μm)	STDEV (μm)
3.8	0.4	20	10	0.7
3.3	0.4	20	12	0.7
2.2	0.4	20	20	2
0.00	0.4	20	23	2
0.00	0.0	0	68	10

Table IV. Experimentally calculated boundary layer thickness as a function of agitation (flow rate, lateral oscillation rate and vibration frequency) on a 46 cm × 61 cm flat stainless steel substrate in the non-traditional cell. Location 1 on the panel.

Pump Flow Rate (L/s)	Osc (osc/s)	Vib (cycles/s)	Ave δ (μm)	STDEV (μm)
0.00	0.0	0	68	10
2.2	0.4	0	38	-
2.2	0.0	20	31	-
2.2	0.1	20	30	-
2.2	0.4	20	20	2
2.2	0.7	20	26	-
2.2	1.0	20	25	-
3.8	0.1	20	12	0.1
3.8	0.4	20	10	0.7
3.8	0.7	20	12	0.5
3.8	1.0	20	13	0.3
3.8	0.4	35	12	1
3.8	0.4	5	13	0.7

Table V. Experimentally calculated boundary layer thickness, demonstrating the effect of panel size, in the non-traditional cell. Location 1 on the panel.

Panel Size (cm × cm)	Pump Flow Rate (L/s)	Osc (osc/s)	Vib (cycles/s)	Ave δ (μm)	STDEV (μm)
31 × 46	0.00	0.0	0	73	-
50 × 50	0.00	0.0	0	47	4
46 × 61	0.00	0.0	0	68	10
50 × 50	3.3	0.4	20	14	1
46 × 61	3.3	0.4	20	12	0.7
31 × 46	3.8	0.4	20	11	0.6
50 × 50	3.8	0.4	20	11	0.3
46 × 61	3.8	0.4	20	10	0.7

Table VI outlines the experimentally determined boundary layer thicknesses as a function of location on the flat stainless steel panel, shown schematically in Figures 5a and 5b for 46 cm × 61 cm and 50 cm × 50 cm substrates, respectively. The boundary layer thickness was uniform across the surface of both substrates; uniformity of the boundary layer thickness aids in deposition thickness uniformity and enables simple processing conditions.

Table VI. Comparison of model predicted boundary layer thicknesses and experimentally calculated boundary layer thicknesses as a function of location on a 46 cm × 61 cm flat stainless steel substrate in the non-traditional cell for a pump flow rate of 3.8 L/s, oscillation of 0.4 oscillations/s and vibration of 20 cycles/s.

Location on Panel	δ (μm) Experimental	STDEV (μm) Experimental	δ (μm) Model
1	10	0.7	10
2	12	0.3	12
3	13	0.7	13
4	12	0.3	11
5	10	0.6	9

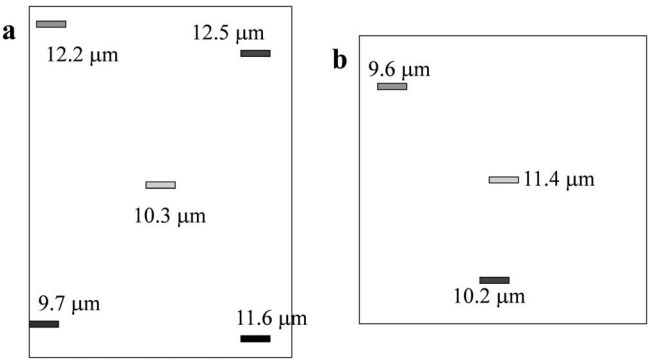

Figure 5. Location of exposed area on a flat substrate for linear polarization curves and consequent calculation of boundary layer thickness in the non-traditional cell for a) a 46 cm × 61 cm flat stainless steel substrate and b) a 50 cm × 50 cm flat stainless steel substrate.

Modeling of boundary layer thickness.—The results of the boundary layer thickness experiments were used to validate a model developed to predict the boundary layer conditions as a function of feature density on a PCB panel in the non-traditional cell. Preliminary model results show good agreement with the experimental results in terms of boundary layer thickness (Table VI). Furthermore, the model predicts how the pump flow rate influences the uniformity of the boundary layer thickness, shown schematically in Figure 6, where flow rates of

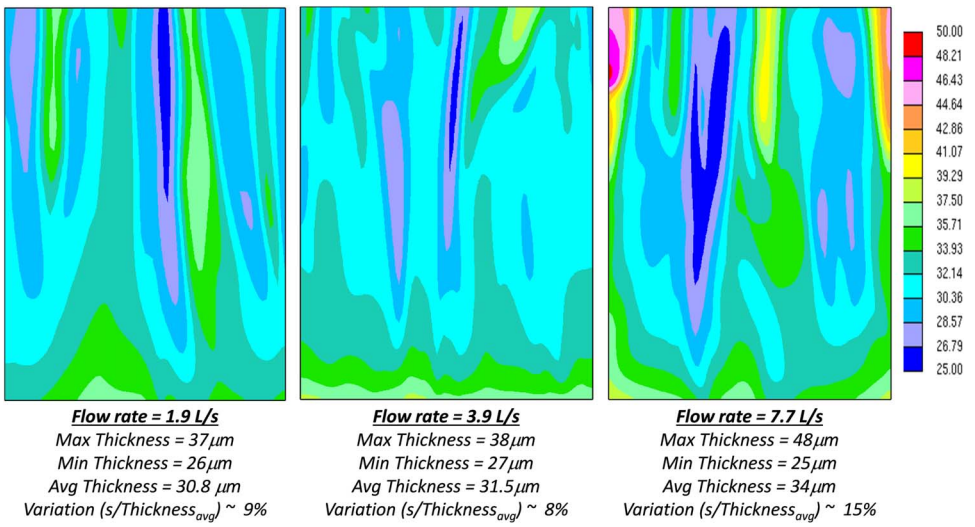

Figure 6. Model prediction of boundary layer thickness as a function of flow rate (1.9, 3.9 and 7.7 L/s) in the non-traditional cell. Flow rate of 3.9 L/s is considered the baseline condition.

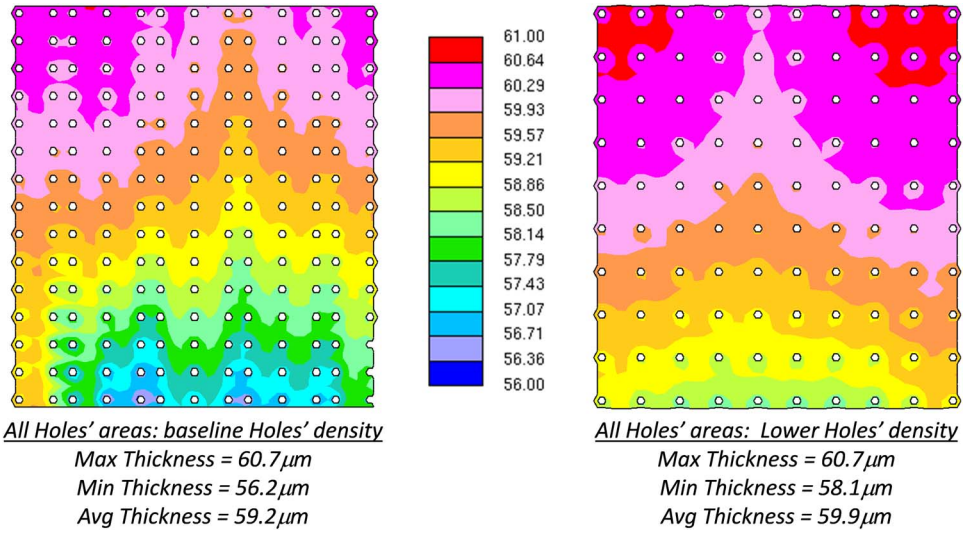

Figure 7. Model prediction of boundary layer thickness as a function of plated through hole density in the non-traditional cell; densities of 195 holes/5.14 cm^2 and 100 holes/5.14 cm^2 were considered. The condition of 195 holes/5.14 cm^2 is considered the baseline condition as was taken from an actual printed circuit board panel.

1.9, 3.9 and 7.7 L/s were utilized as model input parameters. Based on the model output, it is predicted that the solution composition will have a major effect on the thickness of the boundary layer within the non-traditional cell. In terms of pump flow rate, the model predicts minimal change in the boundary layer thickness and distribution variation when increasing the rate from 1.9 L/s to 3.9 L/s (variation of 9% compared to 8%), however, greater variation in the boundary layer thickness results from a further increase in the pump flow rate from 3.9 L/s to 7.7 L/s (8% compared to 15%).

Once a model was created to simulate the flow regime within the non-traditional cell and validated with experimental data, the model was refined to predict the boundary layer conditions as a function of PTH diameter and density. A PCB panel was used to determine representative PTH diameter and spacing for the model input. The area considered for model development was 5.14 cm^2 from a 46 cm × 61 cm panel; the holes located within this array of PTHs serve as the baseline for model input at a diameter of 0.05 cm and a density of 195 holes/5.14 cm^2; a lower feature density of 100 holes/5.14 cm^2 was also considered. The model predicts an average boundary layer thickness of 59.2 μm for the baseline PTH density and 59.9 μm for the lower PTH density. However, the range of boundary layer thicknesses is slightly larger for the baseline condition (maximum boundary layer thickness of 60.7 μm and a minimum thickness of 56.2 μm) when compared to the lower PTH density (maximum boundary layer thickness of 60.7 μm and a minimum thickness of 58.1 μm). These results are shown in Figure 7 (note that the PTH spacing is not necessarily uniform as the baseline condition has a pattern of non-uniform spacing whereas pattern in lower density condition does utilize uniform spacing of the PTHs).

The model also evaluated the effect of PTH diameter on the thickness and uniformity of the boundary layer in the non-traditional cell. The baseline diameter was taken as 0.05 cm; the model also considers PTHs with diameters of 0.1 cm and 0.025 cm. This portion of the model assumes a PTH density of 100 holes/5.14 cm^2 where the holes are evenly spaced. As shown in Figure 8, the model predicts that the average boundary layer thickness decreases with PTH diameter, though the difference between the three cases is small (average boundary layer thickness of: 60.0 μm for 0.1 cm holes, 59.7 μm for 0.05 cm holes and 56.5 μm for 0.025 cm holes), however the maximum thickness of the boundary layer is similar for all three cases (60.9 μm, 60.8 μm and 60.4 μm, respectively). It is noted that the distribution of boundary layer is significantly different at smallest PTH diameter

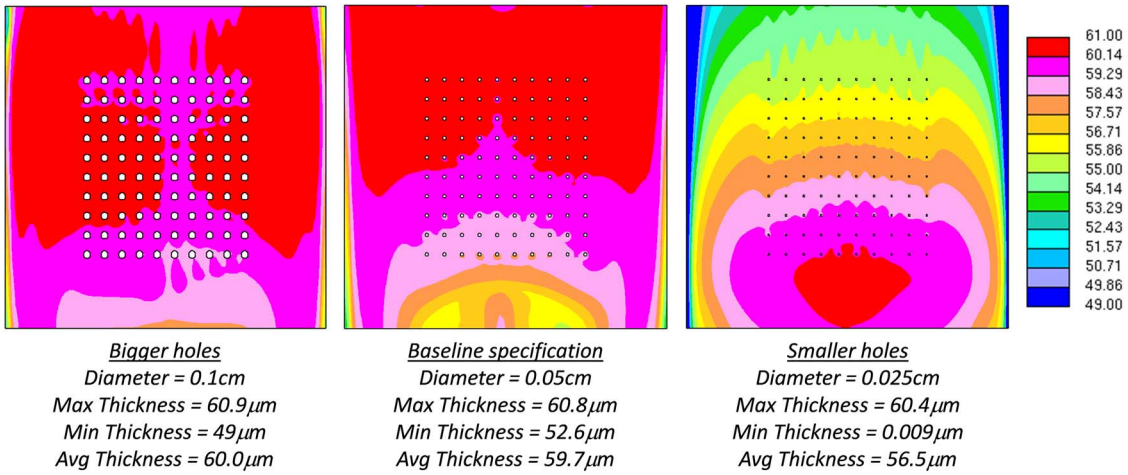

Figure 8. Model prediction of boundary layer thickness as a function of plated through hole diameter in the non-traditional cell. While diameters of 0.1 cm, 0.05 cm and 0.025 cm were considered, 0.05 cm represents the baseline condition, which was determined from an actual printed circuit board panel.

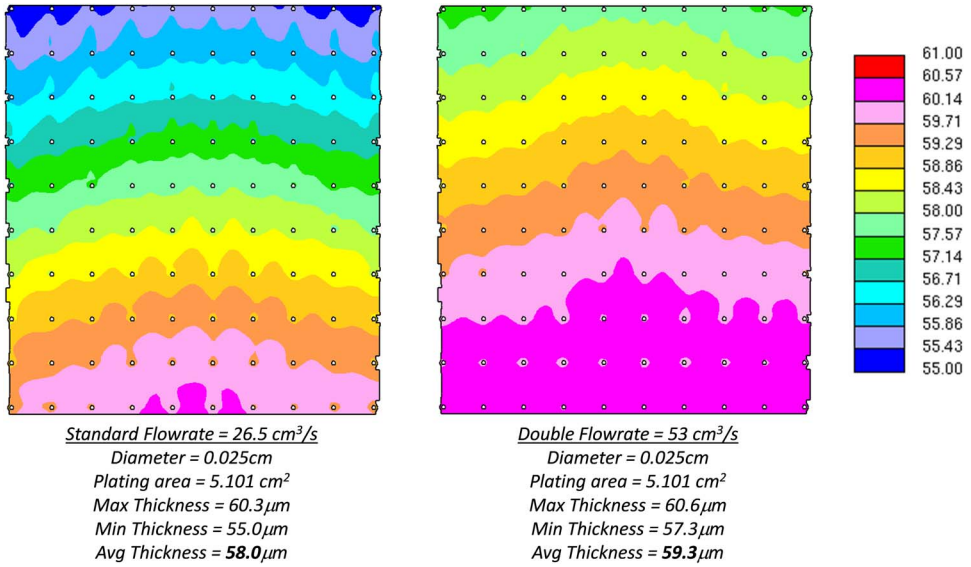

Figure 9. Model prediction of the effect of flow rate on the boundary layer thickness for the smallest diameter plated through hole considered (0.025 cm) in the non-traditional cell.

of 0.025 cm compared to other two cases. This could be due to the significant increasing of the plating area.

The predicted effect of flow rate on the smallest diameter PTH (0.025 cm and PTH density of 100 holes/5.14 cm^2) is shown in Figure 9 for flow rates of 26.5 cm^3/s and 53 cm^3/s. The uniformity of boundary layer thickness is improved with increasing the flow rate. For this PTH diameter and density, there appears to be only a minor effect in the boundary layer condition when doubling the flow rate from 26.5 to 53 cm^3/s.

Conclusions

A non-traditional plating cell was engineered to provide a uniform boundary layer thickness to dampen uneven localized current distributions and promote consequent plating uniformity for full size PCB panels. Delivery of a uniform boundary layer is facilitated by cell geometry, specifically the coupled flow channels and dampening elements utilized to direct the eductor flow in a parallel fashion across the substrate surface. Characterization work has validated both the presence of a thin, uniform boundary layer and consequent plating uniformity in terms of thickness distribution of the deposit.

When considering the boundary layer thickness in the presence of the PTH array, the model predicts a 16% variant in the boundary layer thickness from minimum values to maximum values calculated. The results of this study suggest that patterns on a PCB increase the non-uniformity of the boundary layer thickness; this has been observed in previous research.[10–12] The non-uniformity of the boundary layer thickness of the areas adjacent to the PTHs shows a variation of ~8% which coincides with the variation in the plating thickness on a flat substrate. When considering different PTH densities, a high density of PTHs will cause a greater flow disturbance when compared to lower PTH density, which results in an increase the non-uniformity of the boundary layer thickness. Furthermore, larger PTH diameters (0.1 cm) with the same hole density (100 holes/5.14 cm^2) yields a reduction in plating area and consequently results in increased boundary layer thicknesses. Small diameter PTHs (0.025 cm) are predicted to show more non-uniformity in the boundary layer thickness as well as thinner average thickness values. The model also predicts that increasing the flow rate in the case of the small diameter PTHs helps improve the non-uniformity of the boundary layer condition.

Acknowledgments

Funding for development of this technology is gratefully acknowledged through National Science Foundation (SBIR grant #1057816) and TTM Technologies (Anaheim, CA). Any opinions, findings, and conclusions or recommendations expressed in this material are those of the author(s) and do not necessarily reflect the views of the National Science Foundation. The authors acknowledge Dr. Maria Inman for the diligent review and helpful edits during the preparation of this manuscript. In addition, the funding by the Department of Defense under SBIR Contract No. DASG60-01-C-0056 is gratefully acknowledged.

References

1. U.S. Pat. No. 5,516,412, *Vertical Paddle Plating Cell*, May 14th, 1996.
2. L.E. Gebhart, J. J. Sun, P. O. Miller, and E. J. Taylor, *Electroplating Cell with Hydrodynamics Facilitating More Uniform Deposition across a Workpiece during Plating*, U.S. Pat. 7,553,401, June 30, 2009.
3. L. E. Gebhart and E. J. Taylor, *Method of Operating an Electroplating Cell with Hydrodynamics Facilitating More Uniform Deposition on a Workpiece with Through Holes*, U.S. Pat. 7,947,161, May 24, 2011.
4. L. E. Gebhart and E. J. Taylor, *Electroplating Cell with Hydrodynamics Facilitating More Uniform Deposition on a Workpiece with Through Holes during Plating*, U.S. Pat. 8,226,804, July 24, 2012.
5. L. E. Gebhart, J. J. Sun, P. O. Miller, and E. J. Taylor, *Electroplating Cell with Hydrodynamics Facilitating More Uniform Deposition across a Workpiece during Plating*, U.S. Pat. 8,329,006, December 11, 2012.
6. D.-T. Chin and C.-H. Tsang, *J. Electrochem Soc.*, **125**(9), 1461 (1978).
7. K.-L. Hsueh and D.-T. Chin, *J. Electrochem Soc.*, **133**(1), 75 (1986).
8. K.-L. Hsueh and D.-T. Chin, *J. Electrochem Soc.*, **133**(9), 1845 (1986).
9. B. Q. Wu, Z. Lui, A. Keigler, and J. Harrell, *J. Electrochem. Soc*, **152**(5), C272 (2005).
10. P. Raffelstetter, B. Mollay, B. Van den Bossche, and G. E. Nauer, *J. Electrochem Soc*, **156**(2), D51 (2009).
11. R. Akolkar and V. Dubin, *Electrochem Solid State Lett*, **10**(6), D55 (2007).
12. A. C. West, M. Matlosz, and D. Landolt, *J. Electrochem Soc*, **138**(3) 728 (1991).